TABLE 2 Variation of Constituents in Normal Healthy Bile Samples and Cholestatic Jaundice Samples

Sample	Cholesterol (mg/dl)	Bile Pigments (mg/dl)	Bicarbonate Ions (mg/dl)	Bile Salts (mg/dL)
bN-1	170-195	50-95	28-40	32-66
bN-2	168-205	45-88	32-45	40-60
bN-3	160-185	69-78	40-56	25-45
bN-4	155-180	65-85	38-54	30-58
bCJ-1	412-440	242-322	322-373	129-135
bCJ-2	423-461	205-292	307-327	114-127
bCJ-3	440-476	244-273	346-360	122-140
bCJ-4	413-455	269-292	356-377	130-138

that of normal bile samples and the increased level of bicarbonate ions and bile salts.

The results of the case study have shown a great correlation between the laboratory results and bile diagnosis using microwaves.

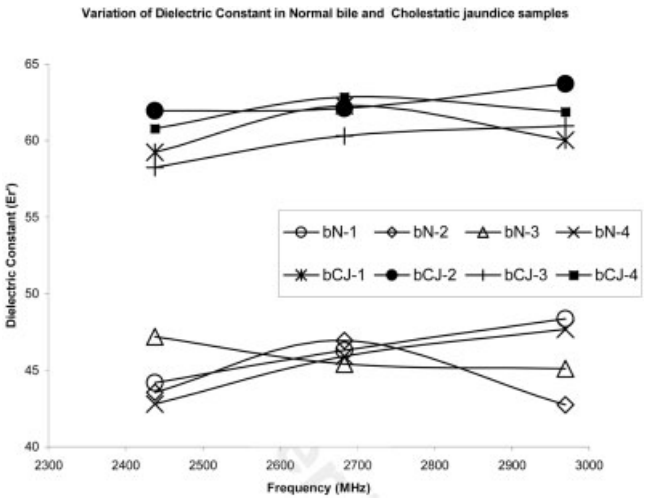

Figure 3 Variation of dielectric constant in normal healthy bile samples and cholestatic jaundice samples

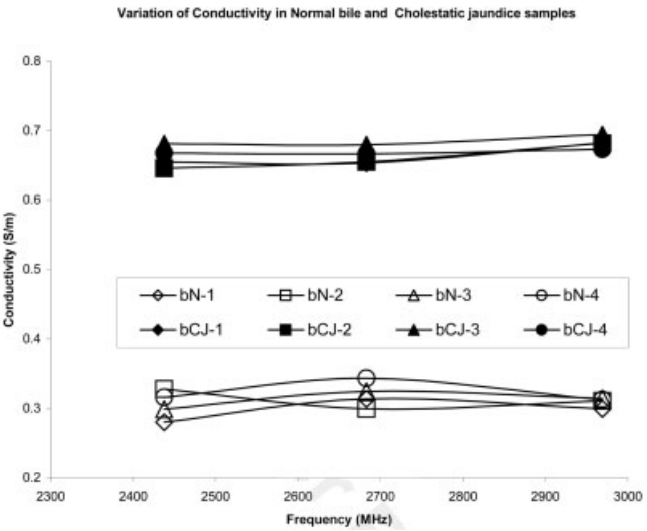

Figure 4 Variation of conductivities in normal bile and cholestatic jaundice samples

6. CONCLUSION

The microwave characterization of the bile samples is done using cavity perturbation technique. The cavity perturbation technique is quick, simple, and accurate and it requires very low volume of sample for measuring the dielectric properties of tissue samples and biological fluids. It is observed that in the specified band of frequencies, there is an appreciable change in the dielectric properties of patient samples with the normal healthy samples. These results prove an alternative in-vitro method of detecting bile abnormalities based on the measurement of the dielectric properties of bile samples using microwaves without surgical procedure.

REFERENCES

1. A. Lauri, R.C. Horton, B.R. Davidson, A.K. Burroughs, and J.S. Dooley, Endoscopic extraction of bile duct stones: management related to stone size, Gut 34 (1993), 1718–1721.
2. "Special Issues," IEEE Trans Microwave Theory Tech 50 (2002).
3. A. Von Hippel, Dielectric and waves, Artech House, Norwood, MA, 1995.
4. S. Gabriel, R.W. Lau, and C. Gabriel, The dielectric properties of biological tissues. II. Measurements on the frequency range 10 Hz to 20 GHz Literature survey, Phys Med Biol 41 (1996), 2251–2269.
5. H.F. Cook, Dielectric behavior of human blood at microwave frequencies, Nature 168 (1951), 247–248.
6. H.F. Cook, The dielectric behavior of some types of human tissues at microwave frequencies, Br J Appl Phys 2 (1951), 295–300.
7. D.K. Ghodgaonkar, V.V. Varadan, and V.K. Varadan, Free space measurement of complex permittivity and complex permeability of magnetic materials at microwave frequencies, IEEE Trans Instrument Measurement 19 (1990), 387–394.
8. D.K. Ghodgaonkar, V.V. Varadan, and V.K. Varadan, A free space method for measurement of dielectric constant and loss tangents at microwave frequencies, IEEE Trans Instrument Measurement 38 (1989), 789–793.
9. W. Barry, A broadband, automated, stripline technique for the simultaneous measurement of complex permittivity and complex permeability, IEEE Trans Microwave Theory Tech 34 (1986), 80–84.
10. Z. Abbas, R.D. Pollard, and R.W. Kelsall, A rectangular dielectric waveguide technique for determination of permittivity of materials at W-band, IEEE Trans Microwave Theory Tech 46 (1998), 2011–2015.
11. K.T. Mathew, Perturbation theory, Encyclopedia of RF and microwave engineering, Vol. 4, Wiley-Interscience, USA, 2005, pp 3725–3735.

WWAN CERAMIC CHIP ANTENNA FOR MOBILE PHONE APPLICATION

Ming-Ren Hsu and Kin-Lu Wong
Department of Electrical Engineering National Sun Yat-Sen University, Kaohsiung 804, Taiwan; Corresponding author: hsumr@ema.ee.nsysu.edu.tw

Received 26 May 2008

ABSTRACT: *A promising compact ceramic chip antenna capable of generating two wide operating bands at about 900 and 2000 MHz for covering GSM850/900/1800/1900/UMTS WWAN (wireless wide area network) operation is presented. The antenna comprises a ceramic chip base of high relative permittivity 40 and small volume 2.5 × 5 × 40 mm^3 (0.5 cm^3) and a simple metal pattern embedded therein. The metal pattern is of an asymmetric T-shape with two different simple radiating arms; no meandering in the metal pattern is used, which is different from the meandered-type metal pattern used in conventional chip antennas. Without meandering in the metal pattern, the possible large coupling between the adjacent portions in the metal pattern can be avoided.*

Large operating bandwidths are hence promising to be achieved. Also, without meandering in the metal pattern, the proposed chip antenna can still occupy a small volume for WWAN operation. The small volume allows it easy for the proposed antenna to incorporate the possible electronic elements such as the speaker and the lens of the embedded camera at the top portion of the system circuit board of the mobile phone to achieve a compact integration. Details of the proposed ceramic chip antenna are presented and studied.
Microwave Opt Technol Lett 51: 103–110, 2009; Published online in Wiley InterScience (www.interscience.wiley.com). DOI 10.1002/mop.24020

Key words: *ceramic chip antennas; internal mobile phone antennas; WWAN antennas; penta-band operation*

1. INTRODUCTION

It has been a demanding requirement for achieving a more compact internal antenna for WWAN operation in the mobile phone. Moreover, multiband operation, usually penta-band operation to cover GSM850/900 (824-894/890-960 MHz) in the antenna's lower band and GSM1800/1900/UMTS (1710-1880/1850-1990/1920-2170 MHz) in the antenna's upper band is demanded for the employed internal antenna in the mobile phone. To meet the requirements, the ceramic chip antenna can be a promising choice, owing to its high relative permittivity of the ceramic chip base that can result in a large decrease in the required antenna volume for a fixed operating frequency [1–7]. However, there are very few or no reported ceramic chip antennas that are suitable to operate as an internal antenna and also capable of GSM850/900/1800/1900/UMTS penta-band WWAN operation in the mobile phone. This is largely because it is not an easy task to achieve two wide operating bands at about 900 and 2000 MHz to cover GSM850/900 and GSM1800/1900/UMTS operation when the antenna volume is greatly decreased.

In this article, we present a promising WWAN ceramic chip antenna for internal mobile phone antenna application. Different from the conventional ceramic chip antenna that usually uses a meandered-type metal pattern embedded in the ceramic chip to achieve a much decreased antenna volume, a simple asymmetric T-shape metal pattern with two radiating arms of different lengths for controlling the two desired wide operating bands at about 900 and 2000 MHz is applied. The meandering in the metal pattern is avoided in the proposed antenna, which reduces the possible coupling between two adjacent portions in the metal pattern; in this case, wide operating bandwidths for GSM850/900/1800/1900/UMTS operation are found to be easily achieved for the ceramic chip antenna. At the same time, much decreased antenna volume ($2.5 \times 5 \times 40$ mm^3 or 0.5 cm^3 only) can still be obtained with the use of the high-permittivity ceramic chip base ($\varepsilon_r = 40$) for the proposed antenna.

The proposed antenna is suitable to be surface-mounted perpendicularly at the top no-ground portion of the system circuit board of the mobile phone. In this case, the antenna shows a low profile of 5 mm only on the system circuit board, which can find applications in thin mobile phones [8, 9]. Details of the proposed ceramic chip antenna are described in the article, and results of the fabricated prototype are presented and discussed. In addition, owing to the compact volume of the proposed antenna, it is promising for it to incorporate the associated electronic elements such as the speaker [10, 11] and the lens of the embedded camera [12, 13] to achieve a compact integration in the mobile phone. Characteristics of the proposed ceramic chip antenna incorporating the speaker and the lens of the embedded camera are also studied.

2. PROPOSED WWAN CERAMIC CHIP ANTENNA

Figure 1(a) shows the geometry of the proposed ceramic chip antenna for WWAN operation in the mobile phone. The antenna is enclosed by a 1-mm thick plastic housing (relative permittivity 3.0 and loss tangent 0.02), which is treated as the housing of the practical mobile phones. The antenna is fabricated using LTCC (low temperature cofire ceramic) [1, 2] technology and occupy a volume of $2.5 \times 5 \times 40$ mm^3. The antenna is surface-mounted at the top edge of the no-ground portion (size 10×40 mm^2) of the system circuit board of the mobile phone with its metal pattern perpendicular to the circuit board. Note that a 0.8-mm thick FR4 substrate (relative permittivity 4.4 and loss tangent 0.0245) of size 40×110 mm^2 is used as the system circuit board in this study. On the back side of the circuit board, there is a printed ground plane (size 40×100 mm^2) considered as the system ground plane of the mobile phone, leaving a no-ground portion of size 10×40 mm^2 at the top of the circuit board. A 50-Ω microstrip line printed on the system circuit board is used for testing the antenna in the study. The microstrip line is extended through the no-ground portion to the soldering point at point B. Inside the no-ground portion, there leaves an unoccupied space of 7.5×40 mm^2 between the chip antenna and the system ground plane, which can be utilized to accommodate the possible electronic elements such as the speaker and the lens of embedded camera (see Fig. 9). Detailed results of the antenna incorporating the speaker and the lens of the embedded camera will be presented and discussed in Figure 10 in the next section.

The antenna mainly comprises a high-permittivity ceramic chip base (relative permittivity 40 and loss tangent 0.002) and an asymmetric T-shape metal pattern embedded therein. Detailed dimensions of the metal pattern inside the ceramic chip are shown in Figure 1(b). The T-shape metal pattern can be divided into three parts: a central strip, a longer arm (Arm 1), and a shorter arm (Arm 2). Both Arm 1 and Arm 2 have a widened open-end portion, which can lead to a more uniform excited surface current distribution at the open end and is helpful for achieving enhanced impedance matching over the desired operating bands [14]. The

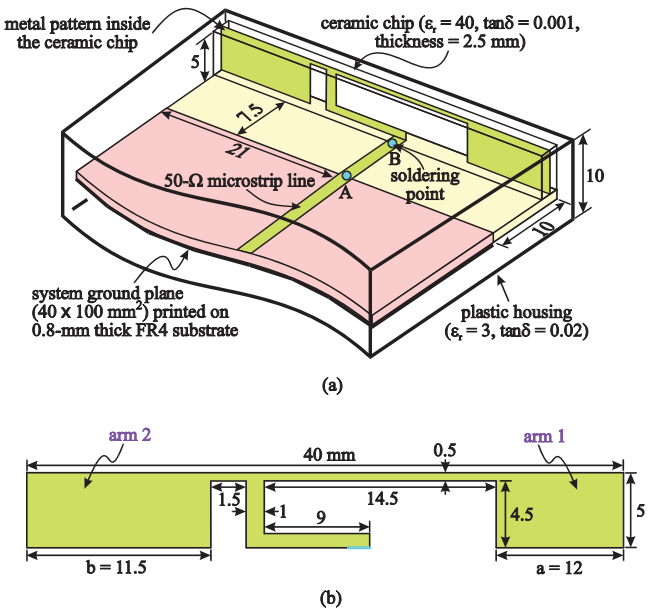

Figure 1 (a) Geometry of the proposed ceramic chip antenna for WWAN operation in the mobile phone. (b) Dimensions of the metal pattern inside the ceramic chip. [Color figure can be viewed in the online issue, which is available at www.interscience.wiley.com]

central strip is bent into a simple inverted-L shape to increase the effective resonant paths for the antenna. There are two major resonant paths controlled by Arm 1 and Arm 2. The longer path has a length of about 46 mm (starting from point A to the open-end of Arm 1) and supports the quarter-wavelength mode at about 900 MHz and a higher-order mode at about 2100 MHz. The shorter path has a length of about 36 mm (starting from point A at the top edge of the system ground plane to the open-end of Arm 2) and generates a quarter-wavelength mode at about 1800 MHz. Note that the high permittivity of the ceramic chip base used in the proposed antenna decreases the required resonant length for the desired quarter-wavelength modes. The excited quarter-wavelength mode of the longer path at about 900 MHz covers GSM850/900 operation, whe reas the higher-order mode of the longer path at about 2100 MHz incorporating the quarter-wavelength mode of the shorter path at about 1800 MHz form a wide operating band to cover GSM1800/1900/UMTS operation.

Also note that by adjusting the lengths (a and b) of the widened open-end portions of Arms 1 and 2, their corresponding excited resonant modes can be controlled. Further, the lengths a and b can control the two modes generated by Arms 1 and 2 to cover GSM1800/1900/UMTS operation, with the quarter-wavelength mode of the longer path at about 900 MHz very slightly affected. This makes it easy to fine-adjust the desired resonant modes for the antenna's lower and upper bands in practical applications. Detailed effects of the lengths a and b on the antenna performance are discussed in Figure 4in Section 3.

3. RESULTS AND DISCUSSION

The proposed ceramic chip antenna with dimensions given in Figure 1 was constructed and tested. Figure 2 shows the measured and simulated return loss for the constructed prototype. The simulated results are obtained using Ansoft HFSS [15], and an agreement between the measurement and simulation is observed. With the definition of 3:1 VSWR (6-dB return loss), which is generally used for internal mobile phone antenna design, the lower band at about 900 MHz controlled by Arm 1 shows an impedance bandwidth of 142 MHz (822–964 MHz), allowing the antenna to cover GSM850/900 operation. The upper band centered at about 2000 MHz controlled by both Arm 1 and Arm 2 shows an impedance bandwidth of 750 MHz (1662–2412 MHz), covering GSM1800/1900/UMTS operation. That is, the proposed antenna can cover GSM850/900/1800/1900/UMTS penta-band WWAN operation.

Figure 3 shows the simulated excited surface current distribu-

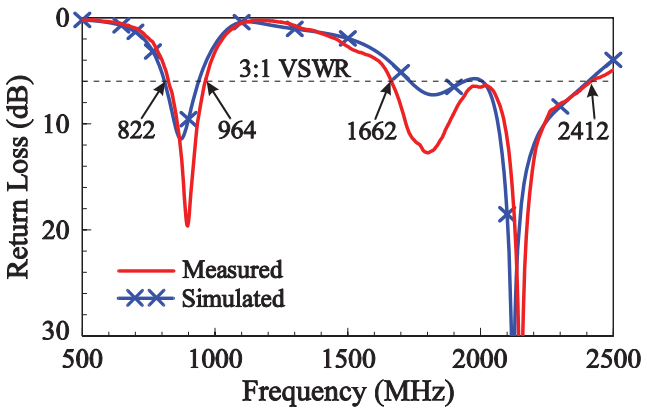

Figure 2 Measured and simulated return loss for the antenna. [Color figure can be viewed in the online issue, which is available at www.interscience.wiley.com]

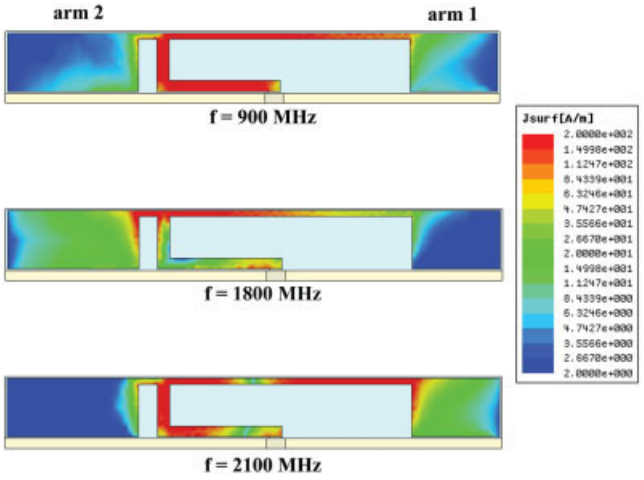

Figure 3 Simulated excited surface current distributions at 900, 1800, and 2100 MHz for the proposed antenna. [Color figure can be viewed in the online issue, which is available at www.interscience.wiley.com]

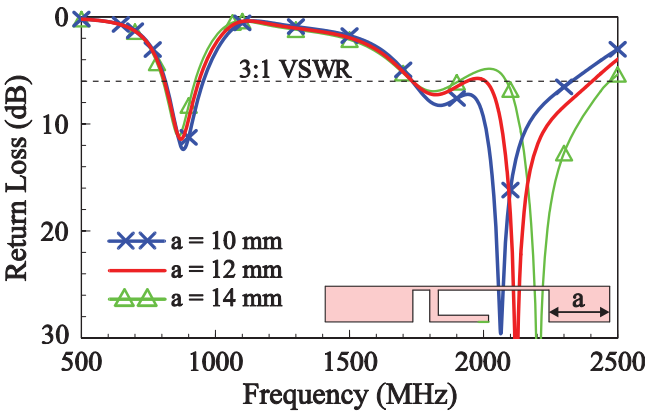

(a)

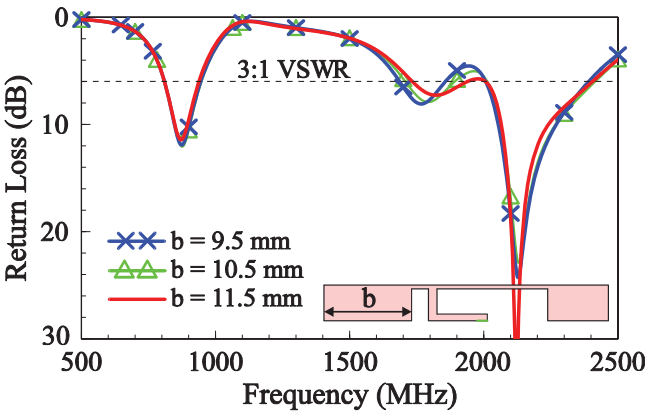

(b)

Figure 4 Simulated return loss as a function of (a) the length a of the widened end portion of arm 1 and (b) the length b for the widened end portion of arm 2. [Color figure can be viewed in the online issue, which is available at www.interscience.wiley.com]

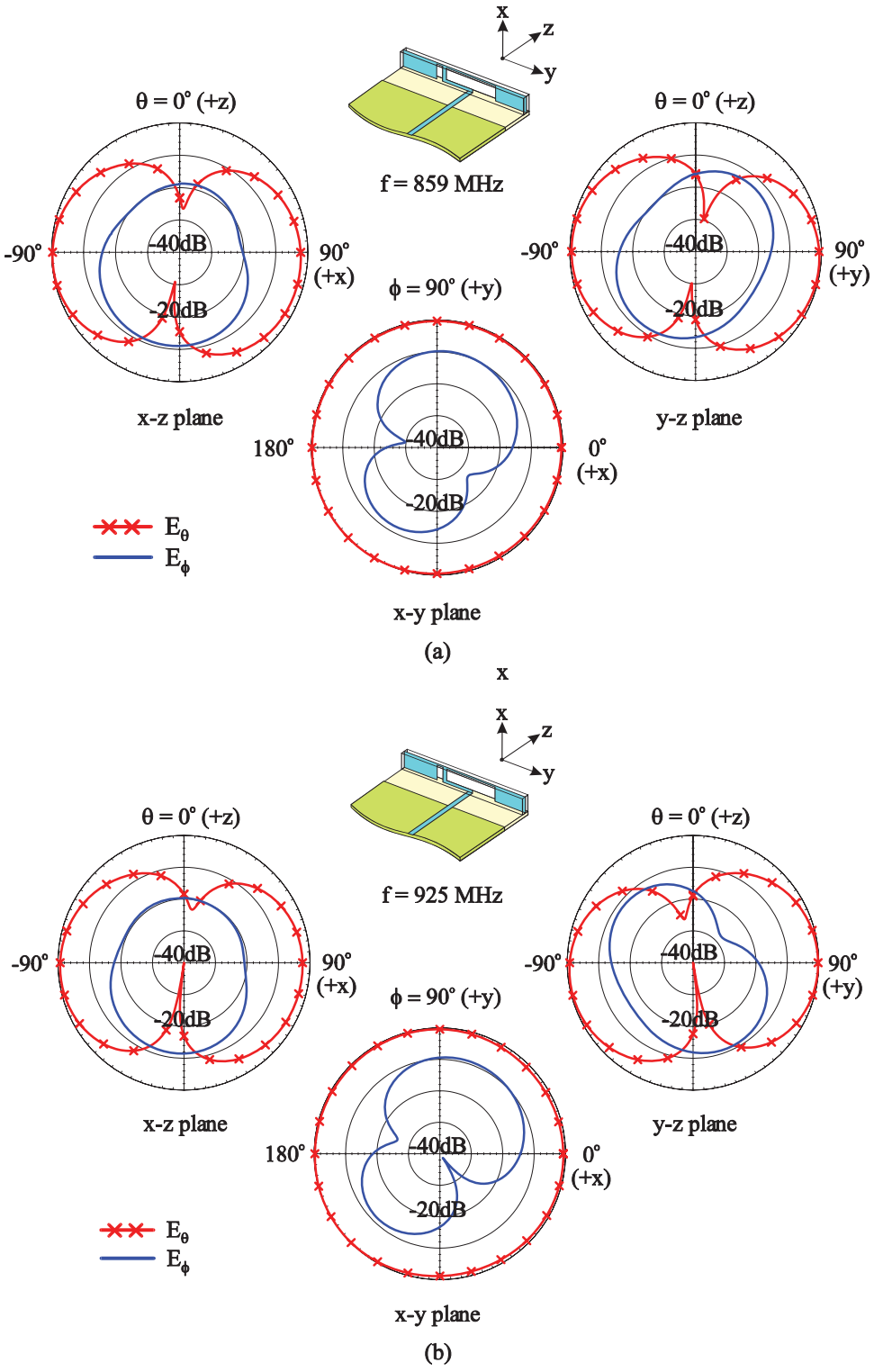

Figure 5 Measured radiation pattern for the proposed antenna. (a) 859 MHz, (b) 925 MHz. [Color figure can be viewed in the online issue, which is available at www.interscience.wiley.com]

tions at 900, 1800, and 2100 MHz for the proposed antenna. At 900 MHz, it is clearly seen that the longer path controlled by Arm 1 dominates the excitation; that is, the antenna's lower band is indeed supported by the longer path or Arm 1. At 1800 MHz, it shows that the shorter path controlled by Arm 2 dominates the first mode in the antenna's upper band. While at 2100 MHz, the longer path again dominates the excitation; that is, the second mode in the antenna's upper band is a higher-order mode generated by the longer path. These excited surface current distributions agree with the discussion in Section 2 for the resonant modes excited for the proposed antenna.

Figure 4 shows the simulated return loss as a function of the lengths a and b of the widened end portions of Arm 1 and Arm 2. Results for the length a varied from 10 to 14 mm are presented in

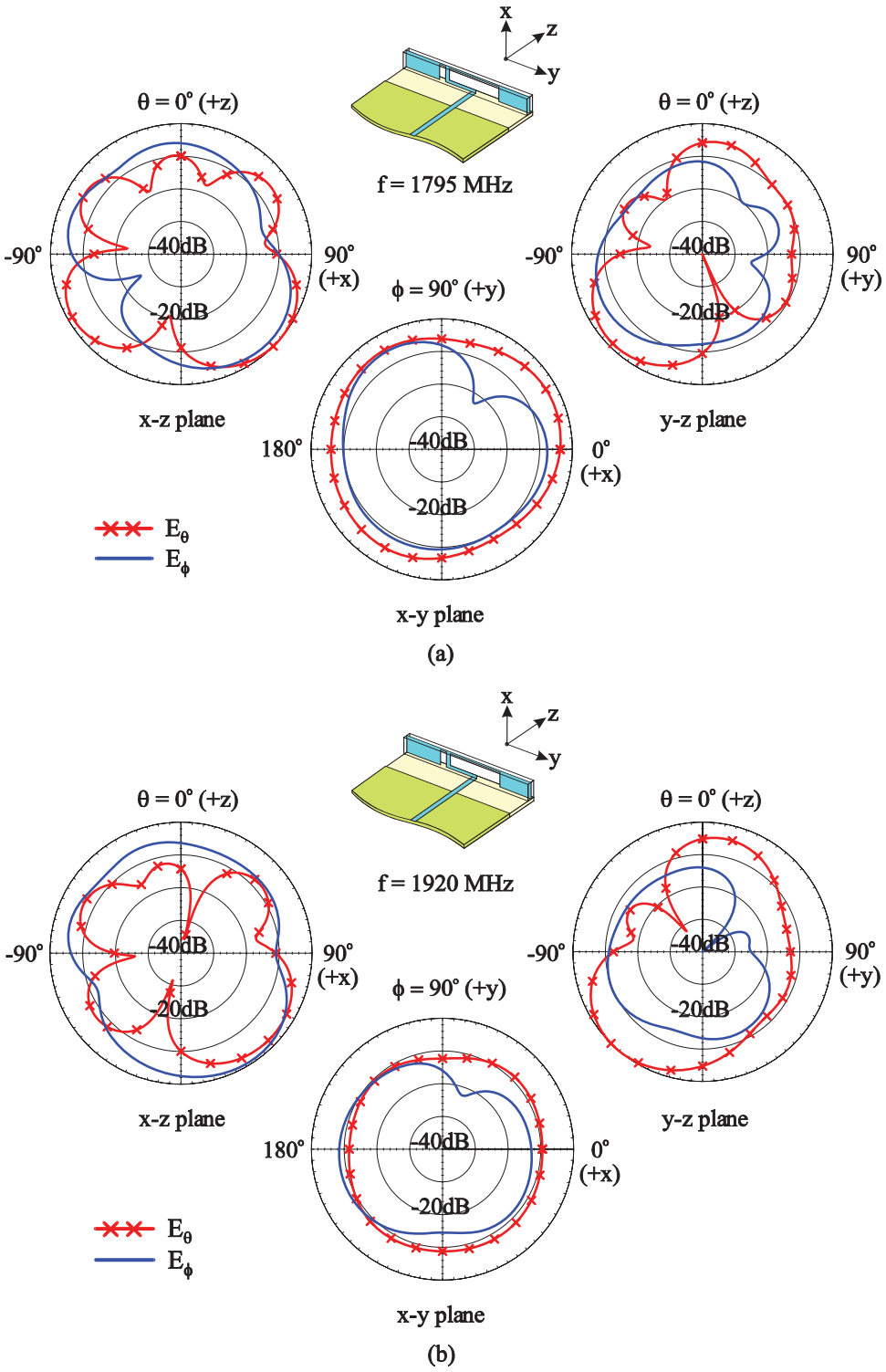

Figure 6 Measured radiation pattern for the proposed antenna. (a) 1795 MHz, (b) 1920 MHz. [Color figure can be viewed in the online issue, which is available at www.interscience.wiley.com]

Figure 4(a); other dimensions are the same as given in Figure 1. Results indicate that when the length *a* is decreased, the quarter-wavelength mode of the longer path at about 900 MHz is very slightly affected, whe reas the higher-order mode of the longer path (the second mode in the upper band) at about 2100 MHz is shifted toward lower frequencies. This is mainly because the effective resonant path for the quarter-wavelength mode of the longer path is about the same for some small variations in the length *a*. However, the higher-order mode of the longer path is more sensitive to the variations in the length *a* (also see the comparison of the surface current distributions at 900 and 2100 MHz), and hence relatively larger shifting for the higher-order mode of the longer path is observed. Figure 4(b) shows the results for the length *b* varied from 9.5 to 11.5 mm. When the length *b* is decreased, the quarter-wavelength mode of the shorter path (the first mode in the upper band) at about 1800 MHz is shifted toward

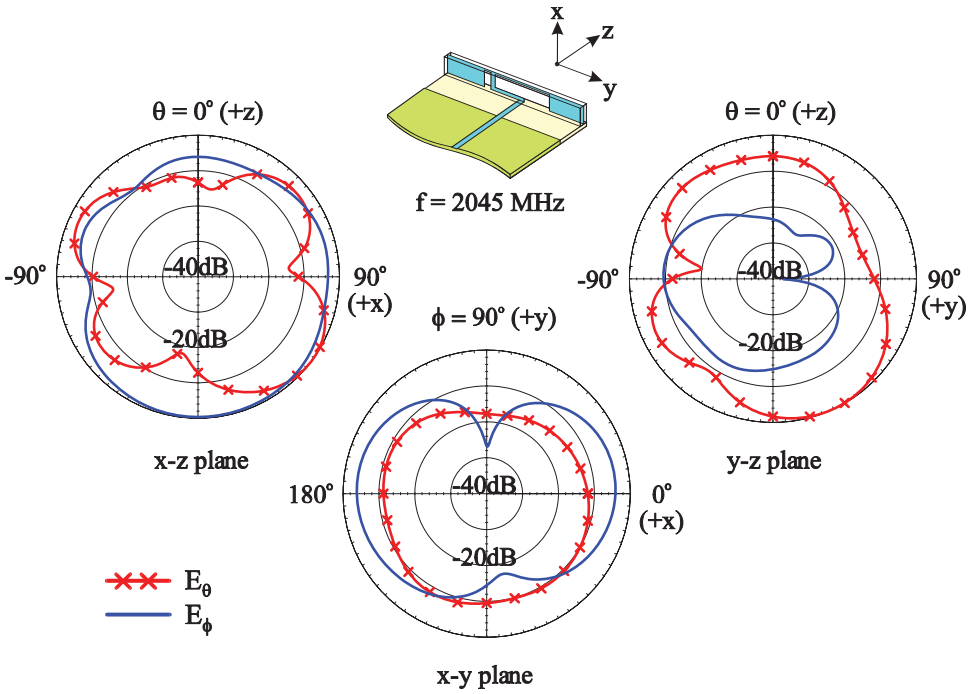

Figure 7 Measured radiation pattern for the proposed antenna at 2045 MHz. [Color figure can be viewed in the online issue, which is available at www.interscience.wiley.com]

lower frequencies. That is because the effective resonant path is lengthened by the decrease in the length *b*. As for the resonant modes at about 900 and 2100 MHz controlled by the longer path, they are very slightly affected. This behavior also agrees with the discussions in Figure 3.

Radiation characteristics of the constructed prototype are also studied. Figure 5 plots the measured radiation patterns at 859 and 925 MHz, the central frequencies of the GSM850 and the GSM900 bands. Monopole-like radiation patterns are observed, which is similar to those of the conventional internal mobile phone antennas for GSM operation. Figure 6 plots the measured radiation patterns at 1795 and 1920 MHz, and those at 2045 MHz are plotted in Figure 7. The frequencies shown in Figures 6 and 7 are the central frequencies of the GSM1800, GSM1900, and UMTS bands. Similar radiation patterns compared with those of the conventional internal mobile phone antennas operated at the corresponding frequencies are also observed. Figure 8 shows the measured antenna gain and the simulated radiation efficiency of the constructed prototype. Over the GSM850/900 band shown in Figure 8(a), the antenna gain is varied from about −0.5 to 1.8 dBi, and the radiation efficiency is varied from about 74% to 90%. Over the GSM1800/1900/UMTS band shown in Figure 8(b), the antenna gain ranges from about 3.7 to 5.1 dBi, and the radiation efficiency is about 63% to 96%. The obtained antenna gain and radiation efficiency are acceptable for practical applications in the mobile phone for WWAN operation.

Figure 9 shows the configuration of the proposed antenna incorporating the possible electronic elements in the mobile phone. A large portion of the lens of the embedded camera is mounted on the front side of the top no-ground portion of the system circuit board, whe reas the speaker partially shielded by the system ground plane is mounted on the back side of the no-ground portion of the circuit board. The simulation model of the speaker is the same as that used in [11] and that for the lens of the embedded camera is shown in Figure 10. The lens can be decomposed into a plastic part for the housing, lid, and holder and a glass part for the

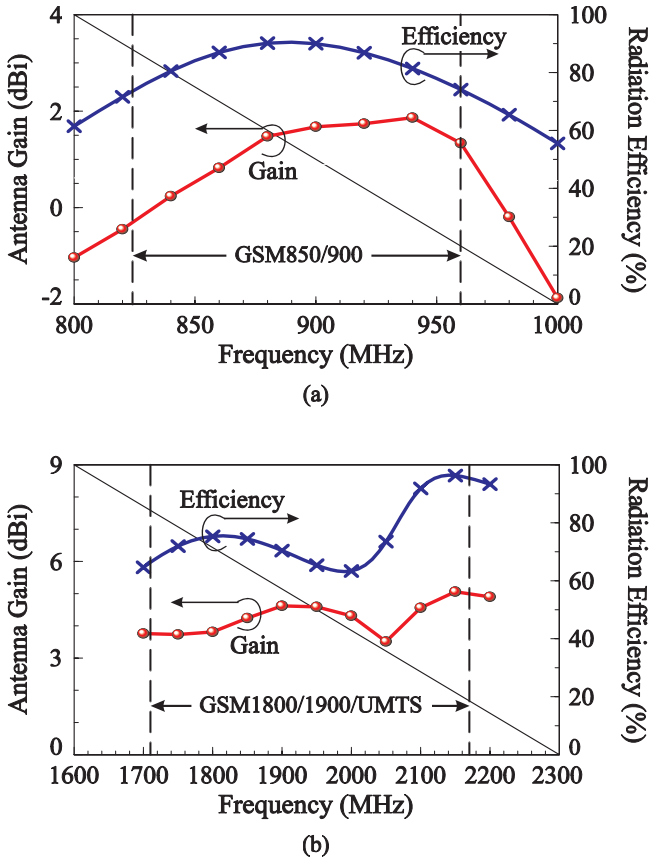

Figure 8 Measured antenna gain and simulated radiation efficiency for the proposed antenna. (a) GSM850/900 band. (b) GSM1800/1900/UMTS band. [Color figure can be viewed in the online issue, which is available at www.interscience.wiley.com]

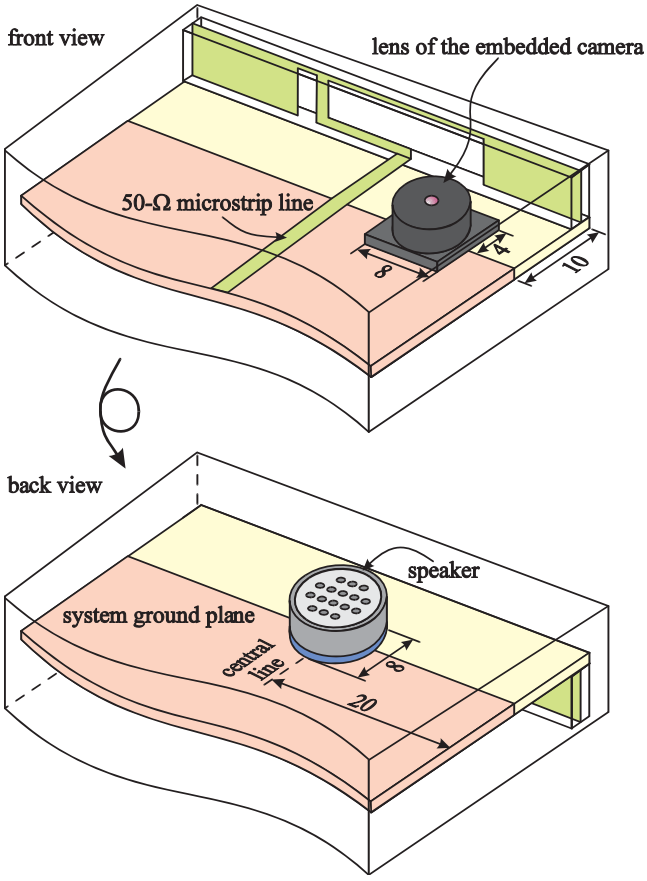

Figure 9 Configuration of the proposed antenna incorporating the speaker and the lens of the embedded camera. [Color figure can be viewed in the online issue, which is available at www.interscience.wiley.com]

lens itself; the relative permittivity and loss tangent of the plastic and glass parts are given in the figure. Figure 11 shows the comparison of the simulated return loss of the proposed antenna with and without the speaker and the lens of the embedded camera. Very small effects on the return loss are seen when the speaker and the lens of the embedded camera are incorporated with the proposed antenna. Figure 12 shows the comparison of the simulated radiation efficiency of the proposed antenna with and without the speaker and the lens of the embedded camera. A decrease in the radiation efficiency is seen. However, the radiation efficiency of

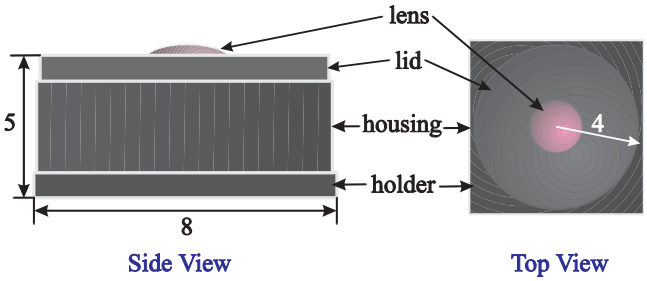

Materials	ε_r	tanδ
Plastic (housing, lid, holder)	3.0	0.02
Glass (lens)	2.5	0.002

Simulation model

Figure 10 Simulation model of the lens of the embedded camera. [Color figure can be viewed in the online issue, which is available at www.interscience.wiley.com]

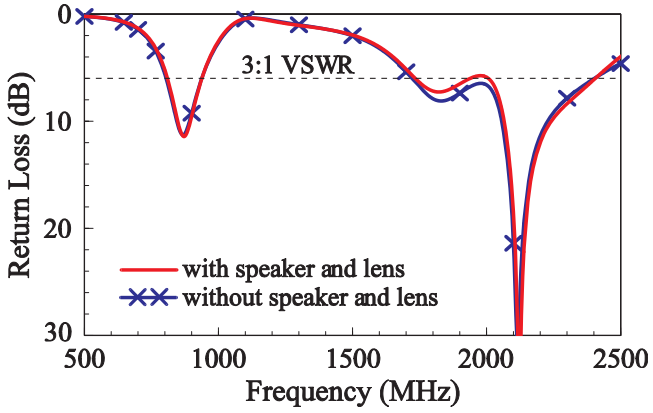

Figure 11 Simulated return loss of the proposed antenna with and without the speaker and the lens of the embedded camera. [Color figure can be viewed in the online issue, which is available at www.interscience.wiley.com]

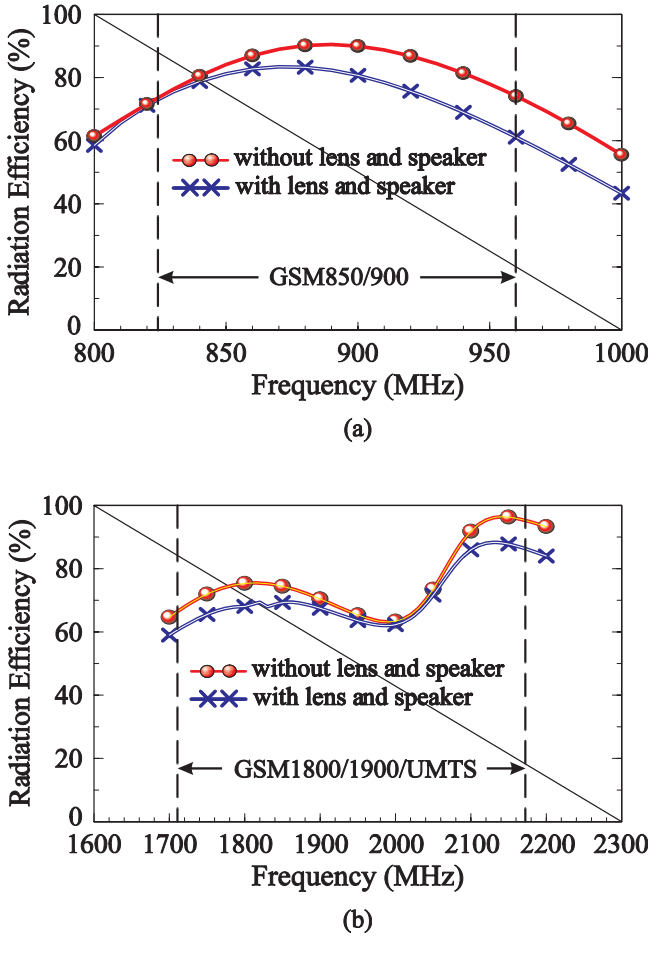

Figure 12 Simulated radiation efficiency of the proposed antenna with and without the speaker and the lens of the embedded camera. (a) GSM850/900 band. (b) GSM1800/1900/UMTS band. [Color figure can be viewed in the online issue, which is available at www.interscience.wiley.com]

the proposed antenna incorporating the speaker and the lens of the embedded camera is still larger than 60% over the desired operating bands, which is promising for practical applications for WWAN operation in the mobile phone.

4. CONCLUSION

A WWAN ceramic chip antenna suitable for mobile phone applications has been proposed and studied. The proposed ceramic chip antenna, although occupying a small volume of $2.5 \times 5 \times 40$ mm^3 (0.5 cm^3) only, can provide two wide operating bands at about 900 and 2000 MHz for covering GSM850/900 and GSM1800/1900/UMTS operation, respectively. By using a high-permittivity ceramic chip base ($\varepsilon_r = 40$) in this study, the occupied volume of the antenna can be greatly reduced. In this case, the use of a simple asymmetric T-shape metal pattern embedded inside the ceramic chip base can result in wide operating bands obtained for WWAN operation for the proposed antenna. For frequencies over the operating bands, good radiation characteristics have also been observed. In addition, the proposed antenna is very suitable to integrate with the associated electronic elements like the speaker and the lens of the embedded camera in the mobile phone, and good radiation efficiency of larger than 60% can still be obtained for the proposed antenna.

REFERENCES

1. Y.D. Kim and H.M. Lee, Design of compact triple-band meander chip antenna using LTCC technology for mobile handsets, Microwave Opt Technol Lett 48 (2006), 160–162.
2. Y.D. Kim, H.Y. Kim , and H.M. Lee, Dual-band LTCC chip antenna design using stacked meander patch for mobile handsets, Microwave Opt Technol Lett 45 (2005), 271–273.
3. J.I. Moon and S.O. Park, Small chip antenna for 2.4/5.8-GHz dual ISM-band applications, IEEE Antennas Wireless Propag Lett 2 (2003), 313–315.
4. D.S. Yim and S.O. Park, Small internal ceramic chip antenna for IMT-2000 handsets, Electron Lett 39 (2003), 1364–1365.
5. W. Choi, S. Kwon, and B. Lee, Ceramic chip antenna using meander conductor lines, Electron Lett 37 (2001), 933–934.
6. K.D. Koo, D.S. Chang, J.S. Sung, and W.S. Lee, Ceramic chip antenna, U.S. Patent No. 6023251, Feb. 8, 2000.
7. K.L. Wong, Planar antennas for wireless communications, Wiley, New York, 2003.
8. K.L. Wong, Y.C. Lin, and T.C. Tseng, Thin internal GSM/DCS patch antenna for a portable mobile terminal, IEEE Trans Antennas Propagat 54 (2006), 238–242.
9. K.L. Wong, Y.C. Lin, and B. Chen, Internal patch antenna with a thin air-layer substrate for GSM/DCS operation in a PDA phone, IEEE Trans Antennas Propag 55 (2007), 1165–1172.
10. C.H. Chang, K.L. Wong, and J.S. Row, Multiband surface-mount chip antenna integrated with the speaker in the mobile phone, Microwave Opt Technol Lett 50 (2008), 1126–1132.
11. C.H. Wu and K.L. Wong, Internal shorted planar monopole antenna embedded with a resonant spiral slot for penta-band mobile phone application, Microwave Opt Technol Lett 50 (2008), 529–536.
12. S.L. Chien, F.R. Hsiao, Y.C. Lin and K.L. Wong, Planar inverted-F antenna with a hollow shorting cylinder for mobile phone with an embedded camera, Microwave Opt Technol Lett 41 (2004), 418–419.
13. C.M. Su, K.L. Wong, C.L. Tang, and S.H. Yeh, EMC internal patch antenna for UMTS operation in a mobile device, IEEE Trans Antennas Propag 53 (2005), 3836–3839.
14. Y.L. Kuo and K.L. Wong, Printed double-T monopole antenna for 2.4/5.2 GHz dual-band WLAN operations, IEEE Trans Antennas Propagat 51 (2003), 2187–2192.
15. Available at: http://www.ansoft.com/products/hf/hfss/, Ansoft Corporation, HFSS Pittsburgh, PA.

MULTIWAVELENGTH SOURCE BASED ON SOA AND EDFA IN A RING-CAVITY RESONATOR

S. Shahi,[1] S. W. Harun,[2] A. H. Sulaiman,[1] K. Thambiratnam,[1] and H. Ahmad[1]

[1] Photonics Research Center, University of Malaya, Kuala Lumpur 50603, Malaysia; Corresponding author: swharun@um.edu.my

[2] Department of Electrical Engineering, University of Malaya, Kuala Lumpur 50603, Malaysia

Received 27 April 2008

ABSTRACT: *A multiwavelength source incorporating a semiconductor optical amplifier (SOA) and a erbium-doped fiber amplifier (EDFA) in a ring-cavity configuration was demonstrated. The multiwavelength source was able to generate more than 13 channels at −27 dBm and above at a SOA bias current of 300 mA and 980-nm pump power of 92 mW. The number of wavelengths generated can be controlled by adjusting the birefringence of the ring cavity using the polarization controllers. The proposed laser has constant channel spacing of 0.8 nm, which is suitable for communication and sensing applications, and shows stable operation at room temperature.* © 2008 Wiley Periodicals, Inc. Microwave Opt Technol Lett 51: 110–113, 2009; Published online in Wiley InterScience (www.interscience.wiley.com). DOI 10.1002/mop.23970

Key words: *multiwavelength fiber laser; semiconductor optical amplifier; ring cavity; loop mirror*

1. INTRODUCTION

Multiwavelength fiber laser sources have recently attracted many interests because of their potential applications in optical component testing, optical fiber sensor networks, and dense wavelength division multiplexing (DWDM) transmission systems [1]. There are many methods available to generate a multiwavelength source; one method is the use of a super-continuum multiwavelength source that is generated by injecting a high repetition rate mode-locked optical pulse into a nonlinear fiber [2, 3]. This, however, requires a complicated configuration with expensive mode-locking device, which is not cost effective. The multiwavelength comb output can also be achieved by utilizing the comb filter in an erbium-doped fiber (EDF) laser at liquid nitrogen temperatures [4, 5]. Unfortunately, because of the homogeneous broadening mechanism of the EDF gain medium, it is difficult to obtain the simultaneous operation of closely spaced multiwavelengths in the EDF laser at room temperature, thus making this method unsuitable for practical applications.

Alternatively, a multiwavelength comb source can be generated using an inhomogeneous gain medium such as semiconductor optical amplifier (SOA) which is capable to effectively suppress the mode competition [6]. However, SOA possesses relatively large insertion loss and high sensitivity to polarization. In this article, a multiwavelength fiber ring laser is demonstrated by incorporating a erbium-doped fiber amplifier (EDFA) into the SOA-based ring laser. The EDFA is used to increase and flatten the gain in the cavity and, as a result, a stable simultaneous multiwavelength laser operation at room temperature can be achieved. Two 3-dB couplers and polarization-maintaining fiber are used to form an interference comb filter, which functions to slice an amplified spontaneous emission (ASE) into multiple wavelengths.